Published in final edited form as:
Biochem J. 2018 November 20; 475(22): 3561–3576. doi:10.1042/BCJ20180750.

Structural basis for the bi-functionality of human oxaloacetate decarboxylase FAHD1

Alexander K. H. Weiss[1,2], **Andreas Naschberger**[3,4], **Johannes R. Loeffler**[2,5], **Hubert Gstach**[6], **Matthew W. Bowler**[7], **Max Holzknecht**[1,2], **Elia Cappuccio**[1,2], **Annabella Pittl**[1,2], **Solmaz Etemad**[1,2], **Theresia Dunzendorfer-Matt**[3], **Klaus Scheffzek**[3,8], **Klaus R. Liedl**[2,5,8], **Pidder Jansen-Dürr**[1,2,8]

[1]University of Innsbruck, Austria; Research Institute for Biomedical Aging Research; Rennweg 10, A-6020 Innsbruck

[2]University of Innsbruck, Austria; Center for Molecular Biosciences Innsbruck (CMBI); Innrain 80-82, A-6020 Innsbruck

[3]Medical University of Innsbruck, Austria; Division of Biological Chemistry, Biocenter; Innrain 80, A-6020 Innsbruck

[4]Medical University of Innsbruck, Austria; Division of Genetic Epidemiology, Schöpfstrasse 41, A-6020 Innsbruck

[5]University of Innsbruck, Austria; Institute of General, Inorganic and Theoretical Chemistry; Innrain 82, A-6020 Innsbruck

[6]University of Vienna, Austria; Faculty of Chemistry; Department of Organic Chemistry; Währinger Straße 38, A-1090 Vienna

[7]European Molecular Biology Laboratory, Grenoble Outstation, 71 Avenue des Martyrs, CS 90181, 38042 Grenoble, France

Abstract

Whereas enzymes in the fumarylacetoacetate hydrolase (FAH) superfamily catalyze several distinct chemical reactions, the structural basis for their multi-functionality remains elusive. As a well-studied example, human FAH domain containing protein 1 (FAHD1) is a mitochondrial protein displaying both acylpyruvate hydrolase (ApH), and oxaloacetate decarboxylase (ODx) activity. As mitochondrial ODx, FAHD1 acts antagonistically to pyruvate carboxylase, a key metabolic enzyme. Despite its importance for mitochondrial function, very little is known about

Correspondence to: Klaus Scheffzek; Klaus R. Liedl; Pidder Jansen-Dürr.

Correspondence should be addressed to K.S. (klaus.scheffzek@i-med.ac.at), K.L. (klaus.liedl@uibk.ac.at) or P.J. (pidder.jansen-duerr@uibk.ac.at).

[8]These authors jointly directed this work.

Competing financial interest

The authors declare not to have any competing financial interest whatsoever.

Author contribution

A.W., A.N., J.L., M.B., M.H., E.C., A.P., S.E., and T.D. performed experiments; A.W., A.N., H.G., and J.L. investigated the protein structure; J.L. and K.L. performed *in silico* simulations; A.W., K.S., K.L., and P.J. designed and supervised the experiments; A.W., A.N., M.B., J.L., H.G., K.S., K.L., and P.J. analysed data and wrote the manuscript.

Europe PMC Funders Author Manuscripts

the catalytic mechanisms underlying FAHD1 enzymatic activities, and the architecture of its ligated active site is currently ill defined. We present crystallographic data of human FAHD1 that provide new insight into the structure of the catalytic center at high resolution, featuring a flexible 'lid'-like helical region which folds into a helical structure upon binding of the ODx inhibitor oxalate. The oxalate-driven structural transition results in the generation of a potential catalytic triad consisting of E33, H30 and an associated water molecule. *In silico* docking studies indicate that the substrate is further stabilized by a complex hydrogen bond network, involving amino acids Q109 and K123, identified herein as potential key residues for FAHD1 catalytic activity. Mutation of amino acids H30, E33, and K123 each had discernible influence on the ApH and/or ODx activity of FAHD1, suggesting distinct catalytic mechanisms for both activities. The structural analysis presented here provides a defined structural map of the active site of FAHD1, and contributes to a better understanding of the FAH superfamily of enzymes.

Introduction

Fumarylacetoacetate hydrolase domain containing protein 1 (FAHD1) is a eukaryotic member of the fumarylacetocetate hydrolase (FAH) superfamily of enzymes. It acts as an oxaloacetate decarboxylase (ODx), catalyzing the decarboxylation of oxaloacetate (OAA) to pyruvate and CO_2 [1]. While not much is known about the physiological role of FAHD1, its reported localization in the mitochondria[2,3] and its ODx function[3] earmark FAHD1 as a potential antagonist of pyruvate carboxylase (PC) at a central node of the tricarboxylic acid (TCA) cycle[4,5]. Consistent with a role of FAHD1 in mitochondrial metabolism, mutational inactivation of the *fahd-1* gene induced mitochondrial dysfunction accompanied by significant locomotion defects in the nematode *Caenorhabditis elegans* [2]. Moreover, shRNA mediated knock-down of *Fahd1* gene expression in human endothelial cells led to a significant decrease in the rates of electron transport and oxidative phosphorylation[6]. Together, these findings imply that FAHD1 supports essential mitochondrial function in eukaryotes.

According to the current model, the flux through the TCA cycle, enabling the complete metabolism of glucose, fatty acids, and amino acids, is partly determined by the availability of the rate limiting metabolites acetyl-coenzyme A (acetyl-CoA) and OAA[7]. The actual concentration of OAA in the mitochondrial matrix is subject to regulation by various metabolic processes, which are not understood to their full extent, including feedback inhibition by intermediate metabolites. Since OAA is known as a potent feedback inhibitor of succinate dehydrogenase (SDH), the key enzyme of the electron transport system (ETS) complex II[8–15], increased levels of OAA may inhibit the flux through the TCA cycle[16]. This finding may explain the inhibition of mitochondrial function observed upon ablation of FAHD1 in nematodes and human cells.

Previous work identified FAHD1 as acylpyruvate hydrolase (ApH) capable to cleave both fumarylpyruvate and acetylpyruvate[17]. In an attempt to explore the structural basis for the observed bifunctionality of FAHD1, we analyzed the structure of its catalytic center and studied structural transitions induced upon binding of its ligand oxalate using X-ray crystallography and molecular modelling approaches. Based on the structural model we

Europe PMC Funders Author Manuscripts

identified key amino acids in the catalytic center. Moreover, the ApH and ODx activities of FAHD1 variants, in which selected key amino acids in the catalytic center were altered, were assessed using enzymatic assays. In conclusion, our findings may suggest distinct catalytic mechanisms for the ApH and ODx activities of FAHD1.

Materials and Methods

Cloning and protein expression

Following RT-PCR amplification, human FAHD1 cDNA (GenBank NP_112485) was inserted into the pET3a vector system (Merck) using restriction enzymes. The amino acid sequence of recombinant FAHD1 protein used for structural studies was identical to the endogenous sequence. The resulting expression vector was introduced into BL21(DE3) *E. coli LysS* cells. Clones were obtained *via* streaking bacteria on LB agar plates using ampicillin / chloramphenicol selection. A single colony was picked and an overnight culture was grown in 1000 ml NZCYM medium, containing the respective selective antibiotics. Bacteria were amplified to an optical density of 0.4 at 600 nm. Protein expression was induced by the addition of isopropyl-1-thio-β-D-galactopyranoside (IPTG, final 1 mM) and incubation was continued for 4 h at 37 °C. Bacteria were harvested *via* centrifugation at 5,000 × *g* at 4°C for 10 min and stored at -70 °C.

Enzyme purification

The recombinant protein was extracted via a four step purification strategy involving ammonium sulphate precipitation, hydrophobic interaction chromatography (HIC), anion exchange chromatography, and gel filtration, as follows: A bacterial cell pellet obtained after protein expression in 1 litre liquid culture was suspended in 10 ml of lysis buffer (50 mM sodium phosphate, 100 mM NaCl, 2 mM DTT, pH 7.0) using ultrasonic waves. The lysate was centrifuged at 5,000 × *g* for 30 min at 4°C. The supernatant was filtered (0.22 μm) and proteins were slowly precipitated using 35% ammonium sulphate final saturation on ice. After centrifugation at 10,000 × *g* for 15 min at 4°C the supernatant was collected, filtered (0.22 μm) and kept on ice. A 5 ml HIC column (GE healthcare) was employed to further purify the protein sample obtained after ammonium sulphate precipitation. Concentrated ammonium sulphate (AS) was used as elution buffer. After introducing a first plateau at 33% AS, an elution gradient (1% / ml slope) was used to separate contaminations from FAHD1 protein. All fractions were analyzed by subsequent SDS polyacrylamide gel electrophoresis (SDS-PAGE). Fractions containing FAHD1 were concentrated, pooled and stored at -70°C overnight. The recombinant FAHD1 protein obtained by HIC did not bind to an anionic exchange column, whereas the majority of bacterial contaminations did. This finding was used to further purify the protein by applying the concentrated eluate of the HIC step onto a MonoQ column (GE Healthcare) and collecting the flow-through on ice. The contaminations were eluted from the column and this procedure was repeated. The collected flow-through was concentrated and stored at -70°C. Size exclusion chromatography using a G75 sephadex column (GE healthcare) was employed as a final purification step in a buffer containing 15 mM Tris-HCl, 50 mM NaCl, and 1 mM DTT. Gel electrophoresis of two preparations followed by silver staining verified the protein's homogeneity; contaminations were barely visible (<< 100 ng/μl).

Crystallization and data collection

Crystallization conditions were adapted from previous work of Manjasetty et al[18]. Recombinant FAHD1 was crystallized by the hanging drop vapour diffusion method at 291 K. Droplets of 1 μl protein solution (≈ 5 μg/μl) plus 1 μl of mother liquid (varying per well, as described below) were set up in 24 well format crystallization plates. The mother liquid was composed of 100 mM Na-HEPES pH 7.5, a range of 5% to 20% PEG 4000 in the four rows, and a range of 10 mM to 200 mM $MgCl_2$ in the six columns. 800 μl of mother liquid were applied to each well. For co-crystallization, FAHD1 protein solution was supplemented with oxalate at a final concentration of 2 mM. Droplets were set up by 1 μl of this solution plus 1 μl of mother liquid of varying composition, as described above. Single crystalline plates appeared after some hours of incubation. Larger crystals were raised in the cold room for several days. Crystals were transferred into a drop of cryo-protectant solution composed of mother liquor supplemented with 25% *glycerol* and were then harvested using suitable sized nylon loops that were mounted on SPINE standard bases. Mounted crystals were flash frozen in liquid nitrogen and shipped within a dry shipping *Dewar* (Taylor-Wharton, CX 100) to the European Synchrotron Radiation Facility (ESRF, Grenoble). X-ray diffraction data were collected by the autonomous ESRF beamline MASSIF-1[19,20] using automatic protocols for the location and optimal centring of crystals[21,22]. Strategy calculations accounted for flux and crystal volume in the parameter prediction for complete data sets. All data were processed using the automatic pipelines at the ESRF[23]. The dataset of the *ligated* structure was reprocessed manually by using the software XDS[24].

Structure solution and refinement—The *unligated* structure was solved using molecular replacement with the software Molrep[25] using the previously solved FAHD1 structure available in the PDB (1saw)[18] as search model. Multiple cycles of manual rebuilding using Coot[26,27] followed by reciprocal space refinement with Refmac5[28] were carried out until the R_{free} value dropped to 20%. Data qualities of *unligated* and *ligated* crystals were assessed by the program Xtriage[29]. In the *ligated* dataset pseudo-merohedral twinning (h, -k, -l) and pseudo translation was detected (see below). The *ligated* structure was solved by molecular replacement with Molrep which placed eight FAHD1 molecules into the asymmetric unit (ASU). Since we deal with both pseudo translation and twinning in the ASU we generated an R_{free} set that was selected in thin shells at different resolutions using the program Sftools of the CCP4i suite[30] in order to minimize correlations of intensities between the R_{work} and R_{free} set. After rigid body refinement with Refmac5 additional positive density was observed in a previous unresolved region near the catalytic site. The model was completed within this region using the automatic model building software Buccaneer in model-extension mode. Multiple cycles of real space refinement in Coot and reciprocal space refinement in Refmac5 were carried out. After placement of the magnesium ion in all the catalytic centres of the eight molecules in the ASU we realized the presence of additional positive density which could not be explained by addition of solvent molecules. Oxalate was built into the unexplained density followed by additional refinement steps (including occupancy refinement). All eight ligands within the ASU could explain the density satisfactory with RSCCs varying between 0.94 and 0.98. Further rounds of real and reciprocal space refinement were carried out until R_{free} value stuck at 29 %. Twin refinement in Refmac5 was used which resulted in an R_{free} value drop to finally 21 %, although the map

improved only moderately. Validation of both structures was done using the program MolProbity[31] and the PDB validation server (https://validate-rcsb-1.wwpdb.org/). Composite omit maps were calculated using Phenix software suite[29].

Enzyme activity assay

ODx and ApH activities of recombinant human FAHD1 protein and selected point variants were tested via a 96 well plate assay: Buffer conditions were set to 50 mM Tris-HCl, 100 mM KCl, and 1 mM $MgCl_2$ at pH 7.4. Substrates oxaloacetate (bought from Sigma-Aldrich, order-ID O4126) and acetylpyruvate (synthesized by HG) were dissolved in assay buffer fresh at the start of each experiment. After 10 min of protein incubation (5-10 μg in 285 μl volume per well at room temperature), 15 μl of 20 mM substrate solution was added, to result in a final substrate concentration of 1 mM in 300 μl, corresponding to 300 nmol per well. The decrease of substrate concentration was observed at 255 nm wavelength via a plate reader at 25 °C. Enzyme activity and kinetic parameters were obtained via the initial reaction rates.

Statistical analysis—Experiments were performed in triplets (n = 3) with independent protein preparations. Data analysis was performed using GraphPad PRISM version 5 (www.graphpad.com). Presented data is the mean and standard deviation within 95 % confidence interval. Statistical comparisons of hFAHD1 variant activities with respect to the wild-type were performed using one-tailed Student's t-test (* $p < 0.05$, ** $p <$ b 0.01, *** $p < 0.001$).

***In silico* simulation—**The crystal structures were protonated using MOE protonate3D[32] and visually reviewed with special attention to different protonation states of amino acids and disulfide bridges. All simulations were performed using AMBER14[33]. The *unligated* and the *ligated* structures were hydrated properly[34] and the protein parametrization was set up using the AMBER-ff14SB force field. Van der Waals, bond-length, bond-angle and the torsion force field parameters for oxalate were taken from GAFF. Partial charges were estimated using the RESP method and electrostatic parameters were calculated using Gaussian[35] at HF/6-31G level. To simulate solvation, the proteins were put into a cubic water box of TIP3P[36] water molecules with 10 Å minimal wall distance using tleap. After equilibration, the production runs of the molecular dynamics (MD) simulations were performed in the isothermal-isobaric ensemble (NPT) with periodic boundary conditions (PBC). The long range electrostatic interactions were treated using particle mesh Ewald sum (PME). The temperature was regulated using the Langevin thermostat and the pressure was kept constant using the Berendsen barostat.

QM/MM docking and geometry optimization

QM/MM geometry optimisations were performed using the Schroedinger sofware suite [Release, S., 2014. 2: Maestro, version 9.8. Schrödinger, LLC, New York, NY]. Virtual ligands oxaloacetate and acetylpyruvate were modelled by augmenting the oxalate ligand in the ligated structure of the experimental dataset. For the optimization the QM region was chosen to contain the ligand, the magnesium cofactor, identified key amino acid sidechains, and the water molecules in the binding pocket. The QM level was described *via* DFT/

B3LYP[37], using the 6-31G* correlated double-zeta basis set. The MM level was described *via* OPLS 2005, using restrained to ensure no conformational changes.

Results

Crystal structures

Human recombinant FAHD1 was crystallized and its structure determined by X-ray crystallography (see Methods), at a resolution of 1.56 Å. Tab. 1 and Tab. 2 cover the data collection statistics and the refinement statistics of the models submitted to the PDB database (6FOG, 6FOH). We were able to collect structural data for the FAHD1 protein in complex with its cofactor Mg^{2+} (referred to hereafter as the *unligated* enzyme) (Fig. 1a). Upon co-crystallization with oxalate, a competitive inhibitor of both prokaryotic and eukaryotic ODx enzymes[3,38,39], we obtained structural data at high resolution for FAHD1 in complex with oxalate (PDB: 6FOG, 1.94 Å) (referred to hereafter as the *ligated* enzyme) (Fig. 1b). In the *unligated* structure (PDB: 6FOH), we find that the first five N-terminal residues are unresolved in chain A. In chain B the first seven N-terminal residues are not resolved. All C-terminal residues are resolved in chain A and chain B. In the *ligated* structure (PDB: 6FOG), we find that the first five N-terminal residues unresolved for the chains A, B, G and H. The first seven N-terminal residues are not resolved in chain E, and the first eight N-terminal residues are unresolved for the chains C, D and F. The numbers of unresolved C-terminal residues counted from the very C-terminus is 1 for the chains A and F, and 2 for chains B, E, G and H. All C-terminal residues in the remaining chains C and D are resolved. The catalytic center of FAHD1 is outlined in detail further below.

While the resolution of a previously described structure (PDB: 1saw[18], 2.2 Å) was improved, the region in between residues D29 and L39 is also not resolved in the electron density presented here for the *unligated* crystal (PDB: 6FOH, 1.56 Å), due to apparent structural disorder. Consequently, we find that in the *unligated* structure, the active site of the protein is solvent-accessible, whereas in the *ligated* structure it is not: Superposition of the *unligated* and *ligated* structures revealed oxalate associated conformational transitions in FAHD1 (Fig. 1c), characterized by the appearance of a the previously undefined *N*-terminal structural segment (referred to as the *'lid'* hereafter) in the electron density map. Together, the *ligated* and *unligated* structures obtained in this study provide a structural definition of the catalytic center of FAHD1, as described in detail below.

The catalytic center of FAHD1—The substrate binding site of both the *ligated* and *unligated* FAHD1 is defined in space by the side chains of key amino acids including G24, R25, K47, E71, E73, D102, R106, Q109, K123, and T192 (Fig. 2a). Octahedral coordination of magnesium is established by three water molecules (W^1, W^2 and W^3 in Fig. 2a) and the side chains of amino acids E71, E73, and D102. Bidentate ligand binding substitutes two water molecules (W^1, W^3) (Fig. 2b). We find that FAHD1 exhibits the evolutionary conserved FAH domain[5], that is comprised of three conserved protein regions, folded by two major hydrogen bond networks spanned by K47-D102-K123 and E71-R106-Q109 side chains (Fig. 2c). Previous work showed that both Mg^{2+} and Mn^{2+} are suitable cofactors to enable FAHD1 catalytic activity (*in vitro*), whereas other divalent metal ions are not[5,17]. In

agreement with a previously described structure (PDB: 1saw[18], 2.2 Å), we find that the protein monomers form dimers that are connected via two magnesium and one chloride ion, as we grew the crystals in the presence of $MgCl_2$ (see Methods). Each monomer features as series of ß-sheet structures that form a barrel-like substructure, comprised of the three major conserved regions of the FAH superfamily[5]. The enzyme's cavity is enclosed in this barrel motif. We find that the magnesium cofactor features octahedral coordination, associating with both water molecules and key amino acid side chains.

Moreover, a previously ill-defined *N*-terminal structural segment is resolved. We observed a change in the backbone orientation of G24 and R25, that suggests a peptide backbone-flip mechanism[40,41] (Fig. S1 and Fig. S2). Subsequently, amino acid side chains of H30 and E33 are positioned in proximity of the Mg^{2+} cofactor, forming a dyad that stabilizes a water molecule (W^4) via hydrogen bonding (Fig. 2b). Both the backbone flip and subsequent appearance of the lid domain are fully supported by electron density maps (Fig. S2 and Fig. S3). The observed structural changes suggest a model of how the *unligated* enzyme acquires catalytic competence. Data shown in Fig. S3b further suggest electronic repulsion of the backbone oxygen of glycine by oxalate as driving force behind the observed structural transition, including the concomitant rearrangement of the R25 side chain. The available data suggest lid closure upon binding of oxalate to the magnesium cofactor[42], and *in silico* simulation (Fig. S1) revealed that these features remain stable over time. Molecular dynamics simulations further revealed that the removal of oxalate from the binding pocket almost instantly results in an increased flexibility of the protein (not shown), whereas the *ligated* structure remains rigid during the full period of simulation.

The key amino acids forming the catalytic center of FAHD1—The relative position of key amino acid side chains and their interactions in the *unligated* and *ligated* structures are displayed as a chemical sketch shown in Fig. 3. Three carboxylates (E73, E71, and D102) and three water molecules constitute the inner coordination sphere of the cofactor. In both structures, two distinct hydrogen bond networks (as indicated by short heteroatom distances) are established by the K47-D102-K123 and E71-R106-Q109 side chains, respectively. In the *unligated* structure, water molecule W^1 connects the catalytic center to the G24 backbone carbonyl of the lid domain. Upon binding of oxalate space is occupied by the ligand next to G24 carbonyl oxygen (Fig. S2 and Fig. S3), which as a consequence performs a peptide-flip due to repulsive forces. Due to this structural change in the start of the *N*-terminal lid domain, a reversal of the local hydrogen bond network is induced: the hydrogen bond acceptor character of the G24-R25 amide bond (backbone) in the *unligated* structure is replaced by a hydrogen bond donor character, which in the *ligated* structure forms a hydrogen bond to the carboxyl group of the ligand (Fig. 3b). The structured lid domain reveals a short two-turn helix, including H30 and E33, in ideal disposition to establish a catalytic dyad (displayed in blue in Fig. 3b). Supported by the Mg-complexed E71 carboxylate, the catalytic dyad appears to direct a water molecule towards the inner coordination sphere of the cofactor, where it remains directionally oriented and stabilized for catalytic function through extensive hydrogen bonding (displayed in blue in Fig. 3b, W^4). Whereas previous work has shown that mutation of E33 and/or H30 to alanine resulted in a significant reduction of ODx activity[3], the effect of these variants on ApH activity were not

studied so far. Of note, we found that replacement of either E33 or H30 by alanine in FAHD1 completely abrogated its ApH activity (Fig. 4, Tab. 3, Fig. S4). The differential effect of these variants on ApH vs. ODx activity is consistent with the requirement of a directed water molecule for hydrolysis of acylpyruvates, whereas the role of such water molecule for a decarboxylation reaction is not obvious (see also below). These findings suggest an important role of the lid domain for both the hydrolase and decarboxylase activities of FAHD1. Similar experiments have been conducted, to investigate the two hydrogen bond networks spanned by the K47-D102-K123 and E71-R106-Q109 side chains. Replacement of the key amino acids D102 and R106 by alanine also resulted in a complete loss of catalytic activity of the enzyme[3] (Fig. 4, Tab. 3). To address the potential role of K123 for FAHD1 activity, a K123A mutant enzyme was produced and tested for ApH as well as ODx catalytic activity. These experiments revealed that K123 is essential for both known catalytic activities of FAHD1, because both ODx and ApH activity were abolished in mutant K123A (Fig. 4, Tab. 3). Similar results have been reported for the ODx activity of the prokaryotic FAH superfamily member Cg1458[38,43].

Discussion

FAHD1 was characterized as a bi-functional enzyme, catalyzing decarboxylation of oxaloacetate[3] as well as hydrolyzation of acylpyruvates[17]. These enzymatic processes require different chemical mechanisms. Of note, the result of the C^3-C^4 cleavage is an identical Mg^{2+} pyruvate-enolate complex in ODx as well as ApH catalysis. In addition, hydrolysis requires a nucleophilic attack by a hydroxyl ion, to prepare for C^3-C^4 bond cleavage. A comparison of the *unligated* and *ligated* FAHD1 enzyme reveals a previously unknown structural transition. We identified a peptide flip[40,41] involving amino acids G24 and R25, which initiates the folding of a two-turn helical protein subdomain (as part of the referred ‘lid’ structure) followed by a global change in the architecture of the catalytic site. An *N*-terminal loop domain, referred to as the “lid”, becomes structured and concludes the cavity, while stabilizing the ligand. A catalytic mechanism involving a flexible lid structure was also proposed for the prokaryotic ODx Cg1458[38,43] of *Corynebacterium glutamicum*, however, enolization of substrates, as proposed for Cg1458[38], is not supported by residues constituting the FAHD1 catalytic center. Of note, the “lid” contains the functionally important amino acids H30 and E33 which are repositioned upon oxalate binding and stabilize a water molecule (W^4) adjacent to the ligand. Disruption of the potential catalytic triad H30/E33/W^4 by replacement of H30 and/or E33 by alanine revealed different requirements of FAHD1 for both reactions. The ability of FAHD1 to catalyse OAA decarboxylation was significantly diminished but not abrogated in these variants. These findings suggest a model for the differential capability of FAHD1 to cleave both substrates, in which the catalytic triad H30/E33/H_2O is essential for the hydrolase activity but largely dispensable for the decarboxylase activity of the enzyme. Moreover, replacement of a lysine residue (K123) by alanine caused a dramatic loss of both ApH and ODx activity, strongly supporting a key role of K123 in the catalytic activity.

We propose that the result of the C^3-C^4 cleavage is an identical Mg^{2+} pyruvate-enolate complex (Mg^{2+}-PY^{2-}) in ODx (Fig 5a) as well as ApH catalysis (Fig. 5b). In addition, hydrolysis requires a nucleophilic attack by a hydroxyl ion, to prepare for C^3-C^4 bond

cleavage. Based on these observations along with pre-existing knowledge about conformational and chemical properties of the substrates in solution, we propose distinct mechanisms for both catalytic properties of FAHD1, as outlined in the following section.

Proposal of a FAHD1 decarboxylase mechanism

Performing *in silico* docking experiments based on the ligated structure, we find that the C^4 carboxylate of oxaloacetate rotated along the C^3-C^4 bond, supported by extensive hydrogen bonding to the Q109-carbamoyl group (O=C-NH···-OOC) (as part of the major E71-R106-Q109 hydrogen bond network) (Fig. 5a, left panel). Subsequently, we suggest that the C^3-C^4 bond cleaves under liberation of carbon dioxide. The remaining resonance stabilized Mg^{2+} pyruvate-enolate complex is quenched to the enol form by K123. According to this model, the primary products of oxaloacetate processing by FAHD1 would be carbon dioxide and pyruvate enol as an intermediate (Fig. 5a, right panel). However, the underlying mechanism of this reaction step is still subject to further investigations.

Proposal of a FAHD1 hydrolase mechanism

Hydrolysis of acylpyruvates implicitly requires a hydroxyl nucleophile for attack on the acyl carbonyl group. It is reasonable to assume that the H30 / E33 dyad is competent to generate such a nucleophile upon deprotonation of the directional oriented cavity-water (Fig. 5b). Our experimental data show that H30 and E33, while increasing to some extent the ability of FAHD1 to catalyze OAA decarboxylation, are absolutely required for the hydrolysis of acetylpyruvate. Substitution of either one of these amino acids disables the ApH mechanism (see above, Fig. 4, Tab. 3, Fig. S4). We suggest that, in analogy to the ODx mechanism, the C^3-C^4 bond is cleaved in analogy to the decarboxylase mechanism under formation of acetic acid and resonance stabilized pyruvate-enolate, which is quenched by K123. Concerning K123, previous work on bacterial acetoacetate hydrolase implied a role for a homologous lysine residue (K116) in an imine-based mechanism of decarboxylation[44]. From analysis of the *ligated* structure presented in this work, we can exclude participation of lysine residue K123 in an imine mechanism, because i) the distance to the electrophilic C^4-carbon center of the FAHD1 substrates is too large (> 4 Å) and ii) no productive trajectory for nucleophilic attack of the acyl-carbonyl group can be adopted by K 123 [45,46].

The above discussed acylpyruvate hydrolase mechanism for FAHD1 reveals close analogy to the mechanism for hydrolysis of fumarylacetoacetate by FAH proposed by Timm et.al.[47]. FAH uses Ca^{2+} to hold its substrate fumarylacetoacatetae, that is stabilized by arginine, lysine and asparagine side chains, mediated by the hydroxyl-groups of proximate tyrosine sidechains. Timm et al.[47] reported a E363-H133-H_2O-E199 hydrogen bond network where a water molecule is kept in position by H133 and E199. Cleavage of the substrate is initiated by formation of a hydroxyl nucleophile produced in deprotonation of water by the imidazole group of H133. The HO^- nucleophile attacks the substrates carbonyl function under formation of a tetragonal alkoxide. This mechanism is distinguished from typical Asp-His-Ser catalytic triads of proteases[47], and similar to the mechanism we hypothesize for the acylpyruvase activity of FAHD1. We find an analogous arrangement in FAHD1 represented by E33-H30-W^4-E71. However, Timm et al.[47] did not report any induced-fit type of lid closure, or any additional important side-chain such as Q109 that we find in our *in silico*

Europe PMC Funders Author Manuscripts

docking studies to be of key importance for the activity of FAHD1. We hypothesize that this is because of the different structure of the substrate, as acetylpyruvate and oxaloacetate feature a smaller carbon chain than fumarylpyruvate, and the required stabilization has to be orchestrated at a different carbon center.

Whereas the proposed general catalytic mechanism for the FAH family[38,43] implies a nucleophilic attack of a hydroxyl to the carbonyl carbon of the substrate, the mechanism deduced from currently available structural information suggests that the C^3-C^4 bond cleavage needs an additional promotion through conformational control and stabilization of the metal complexed substrate molecules. We suggest that this control and stabilization may be provided by amino acids K123 and Q109, however, further experimental work would be required to test this hypothesis. Of note, previous work[38] described that mutation of Q154 in the ODx enzyme Cg1458 (corresponding to Q109 of FAHD1) causes loss of enzymatic activity, which would be consistent with this idea. We suggest that individual mechanisms of these enzymes are dictated by the orientation of the bound substrate in the cavity and the local destabilization by individual sidechains, respectively. Accordingly, a common catalytic mechanism for FAH superfamily members remains elusive[5]. Comparing for example the structure of human FAHD1 protein with human FAH and bacterial Cg1458 (Fig. 6), the high degree of similarity of the hydrolase FAH (Fig. 6a) and the ODx Cg1458 (Fig. 6c) becomes apparent, where FAHD1 (Fig. 6b) seems to be somehow in between. This finding is consistent with a common evolutionary origin of the three genes, as hypothesized before[5].

FAHD1 is an essential regulator of mitochondrial function[2,6], and associated to the regulation of senescence[16]. Its function as ODx renders it as key enzyme in the regulation of oxaloacetate levels, that not only affect the TCA flux, but also regulate the activity of complex II (Succinate dehydrogenase, SDH) in the respiratory chain via inhibition. The presented structure derived results and their analysis enabled a new insight into the decarboxylase and hydrolase mechanisms of FAHD1 and as well as related enzymes of the FAH enzyme superfamily. Based on the presented structural and mechanistic analysis, future work will include the development of small molecule ODx-inhibitors which will allow to dissect the physiological role of FAHD1 in higher organisms including mammals.

Supplementary Material

Refer to Web version on PubMed Central for supplementary material.

Acknowledgements

The authors are very thankful for expert technical assistance by Beáta Kovács-Szalka.

Funding

The work presented in this manuscript has been funded by the European integrated FP6-LIFESCIHEALTH project MiMAGE (http://cordis.europa.eu/project/rcn/74075_en.html) and the Austria Wirtschaftsservice Gesellschaft (AWS), and was supported by a grant from the Austrian Science Funds (FWF) P28975 to K.S.

Data availability, materials and correspondences

Supplementary material is attached to this article online. Material and data is available on direct request. Corresponding authors are addressed by superscript stars.

References

1. Klaffl S, Eikmanns BJ. Genetic and functional analysis of the soluble oxaloacetate decarboxylase from Corynebacterium glutamicum. J Bacteriol. 2010; 192:2604–12. [PubMed: 20233922]
2. Taferner A, Pircher H, Koziel R, Von Grafenstein S, Baraldo G, Palikaras K, et al. FAH domain containing protein 1 (FAHD-1) Is required for mitochondrial function and locomotion activity in C. elegans. PLoS One. 2015; 10:1–15.
3. Pircher H, Von Grafenstein S, Diener T, Metzger C, Albertini E, Taferner A, et al. Identification of FAH domain-containing protein 1 (FAHD1) as oxaloacetate decarboxylase. J Biol Chem. 2015; 290:6755–6762. [PubMed: 25575590]
4. Jansen-Duerr P, Pircher H, Weiss AKH. The FAH Fold Meets the Krebs Cycle. Mol EnzyMol Drug Targets. 2016; 02:1–5.
5. Weiss AKH, Loeffler JR, Liedl KR, Gstach H, Jansen-Dürr P. The fumarylacetoacetate hydrolase (FAH) superfamily of enzymes: multifunctional enzymes from microbes to mitochondria. Biochem Soc Trans. 2018; 46:295–309. [PubMed: 29487229]
6. Petit M, Koziel R, Etemad S, Pircher H, Jansen-Dürr P. Depletion of oxaloacetate decarboxylase FAHD1 inhibits mitochondrial electron transport and induces cellular senescence in human endothelial cells. Exp Gerontol. 2017; 92:7–12. [PubMed: 28286170]
7. Shatalin K, Lebreton S, Rault-Leonardon M, Vélot C, Srere PA. Electrostatic channeling of oxaloacetate in a fusion protein of porcine citrate synthase and porcine mitochondrial malate dehydrogenase. Biochemistry. 1999; 38:881–9. [PubMed: 9893982]
8. Moser MD, Matsuzaki S, Humphries KM. Inhibition of succinate-linked respiration and complex II activity by hydrogen peroxide. Arch Biochem Biophys. 2009; 488:69–75. [PubMed: 19540189]
9. Armstrong C, Staples JF. The role of succinate dehydrogenase and oxaloacetate in metabolic suppression during hibernation and arousal. J Comp Physiol B Biochem Syst Environ Physiol. 2010; 180:775–783.
10. Wojtczak L, Wojtczak AB, Ernster L. The inhibition of succinate dehydrogenase by oxaloacetate. Biochim Biophys Acta-Enzymol. 1969; 191:10–21.
11. Wilkins HM, Koppel S, Carl SM, Ramanujan S, Weidling I, Michaelis ML, et al. Oxaloacetate activates brain mitochondrial biogenesis, enhances the insulin pathway, reduces inflammation and stimulates neurogenesis. Hum Mol Genet. 2014; 137:6528–6541.
12. Kotlyar AB, Vinogradov AD. Interaction of the membrane-bound succinate dehydrogenase with substrate and competitive inhibitors. Biochim Biophys Acta (BBA)/Protein Struct Mol. 1984; 784:24–34.
13. Huang L-S, Shen JT, Wang AC, Berry EA. Crystallographic studies of the binding of ligands to the dicarboxylate site of Complex II, and the identity of the ligand in the “oxaloacetate-inhibited” state. Biochim Biophys Acta-Bioenerg. 2006; 1757:1073–1083.
14. Vinogradov AD, Winter D, King TE. The binding site for oxaloacetate on succinate dehydrogenase. Biochem Biophys Res Commun. 1972; 49:441–444. [PubMed: 4640368]
15. Stepanova A, Shurubor Y, Valsecchi F, Manfredi G, Galkin A. Differential susceptibility of mitochondrial complex II to inhibition by oxaloacetate in brain and heart. Biochim Biophys Acta-Bioenerg. 2016; 1857:1561–1568.
16. Etemad S, Petit M, Weiss AKH, Schrattenholz A, Baraldo G, Jansen-Dürr P. Oxaloacetate decarboxylase FAHD1-a new regulator of mitochondrial function and senescence. Mech Ageing Dev. 2018; doi: 10.1016/Jmad.2018.07.007
17. Pircher H, Straganz GD, Ehehalt D, Morrow G, Tanguay RM, Jansen-Dürr P. Identification of human Fumarylacetoacetate Hydrolase Domain-containing Protein 1 (FAHD1) as a novel mitochondrial acylpyruvase. J Biol Chem. 2011; 286:36500–36508. [PubMed: 21878618]

18. Manjasetty BA, Niesen FH, Delbrück H, Götz F, Sievert V, Büssow K, et al. X-ray structure of fumarylacetoacetate hydrolase family member Homo sapiens FLJ36880. Biol Chem. 2004; 385:935–942. [PubMed: 15551868]
19. Bowler MW, Nurizzo D, Barrett R, Beteva A, Bodin M, Caserotto H, et al. MASSIF-1: a beamline dedicated to the fully automatic characterization and data collection from crystals of biological macromolecules. J Synchrotron Radiat. 2015; 22:1540–1547. [PubMed: 26524320]
20. Nurizzo D, Bowler MW, Caserotto H, Dobias F, Giraud T, Surr J, et al. RoboDiff: combining a sample changer and goniometer for highly automated macromolecular crystallography experiments. Acta Crystallogr Sect D Struct Biol. 2016; 72:966–975. [PubMed: 27487827]
21. Svensson O, Malbet-Monaco S, Popov A, Nurizzo D, Bowler MW, et al. IUCr. Fully automatic characterization and data collection from crystals of biological macromolecules. Acta Crystallogr Sect D Biol Crystallogr. 2015; 71:1757–1767. [PubMed: 26249356]
22. Bowler MW, Svensson O, Nurizzo D. Fully automatic macromolecular crystallography: the impact of MASSIF-1 on the optimum acquisition and quality of data. Crystallogr Rev. 2016; 22:233–249.
23. Monaco S, Gordon E, Bowler MW, Delagenière S, Guijarro M, Spruce D, et al. Automatic processing of macromolecular crystallography X-ray diffraction data at the ESRF. J Appl Crystallogr. 2013; 46:804–810. [PubMed: 23682196]
24. Kabsch W. XDS. Acta Crystallogr D Biol Crystallogr. 2010; 66:125–32. [PubMed: 20124692]
25. Vagin A, Teplyakov A. MOLREP: an Automated Program for Molecular Replacement. J Appl Crystallogr. 1997; 30:1022–1025.
26. Emsley P, Cowtan K. Coot: model-building tools for molecular graphics. Acta Crystallogr Sect D Biol Crystallogr. 2004; 60:2126–2132. [PubMed: 15572765]
27. Emsley P, Lohkamp B, Scott WG, Cowtan K. Features and development of Coot. Acta Crystallogr Sect D Biol Crystallogr. 2010; 66:486–501. [PubMed: 20383002]
28. Murshudov GN, Vagin AA, Dodson EJ. IUCr. Refinement of Macromolecular Structures by the Maximum-Likelihood Method. Acta Crystallogr Sect D Biol Crystallogr. 1997; 53:240–255. [PubMed: 15299926]
29. Adams PD, Afonine PV, Bunkóczi G, Chen VB, Davis IW, Echols N, et al. PHENIX: a comprehensive Python-based system for macromolecular structure solution. Acta Crystallogr D Biol Crystallogr. 2010; 66:213–21. [PubMed: 20124702]
30. Winn MD, Ballard CC, Cowtan KD, Dodson EJ, Emsley P, Evans PR, et al. Overview of the CCP4 suite and current developments. Acta Crystallogr D Biol Crystallogr. 2011; 67:235–42. [PubMed: 21460441]
31. Chen VB, Arendall WB, Headd JJ, Keedy DA, Immormino RM, Kapral GJ, et al. MolProbity: all-atom structure validation for macromolecular crystallography. Acta Crystallogr D Biol Crystallogr. 2010; 66:12–21. [PubMed: 20057044]
32. [Accessed: 13th January 2018] Protonate 3D: Assignment of Macromolecular Protonation State and Geometry. Available at: https://www.chemcomp.com/journal/proton.htm
33. Case DA, Babin V, Berryman JT, Betz RM, Cai Q, Cerutti DS, et al. AMBER14. 2014
34. Wallnoefer HG, Handschuh S, Liedl KR, Fox T. Stabilizing of a Globular Protein by a Highly Complex Water Network: A Molecular Dynamics Simulation Study on Factor Xa. J Phys Chem B. 2010; 114:7405–7412. [PubMed: 20446703]
35. Frisch MJ, Trucks GW, Schlegel HB, Scuseria GE, Robb MA, Cheeseman JR, et al. Gaussian16 Revision A.03. 2016
36. Jorgensen WL, Chandrasekhar J, Madura JD, Impey RW, Klein ML. Comparison of simple potential functions for simulating liquid water. J Chem Phys. 1983; 79:926–935.
37. Lee C, Yang W, Parr RG. Development of the Colle-Salvetti correlation-energy formula into a functional of the electron density. Phys Rev B. 1988; 37:785–789.
38. Ran T, Gao Y, Marsh M, Zhu W, Wang M, Mao X, et al. Crystal structures of Cg1458 reveal a catalytic lid domain and a common catalytic mechanism for the FAH family. Biochem J. 2013; 449:51–60. [PubMed: 23046410]
39. Dimroth P. Characterization of a membrane-bound biotin-containing enzyme: oxaloacetate decarboxylase from Klebsiella aerogenes. Eur J Biochem. 1981; 115:353–8. [PubMed: 7016536]

40. Yan BX, Sun YQ. Glycine residues provide flexibility for enzyme active sites. J Biol Chem. 1997; 272:3190–4. [PubMed: 9013553]
41. Keedy DA, Fraser JS, van den Bedem H. Exposing Hidden Alternative Backbone Conformations in X-ray Crystallography Using qFit. PLoS Comput Biol. 2015; 11 e1004507 [PubMed: 26506617]
42. Csermely P, Palotai R, Nussinov R. Induced fit, conformational selection and independent dynamic segments: an extended view of binding events. Trends Biochem Sci. 2010; 35:539–46. [PubMed: 20541943]
43. Ran T, Wang Y, Xu D, Wang W. Expression, purification, crystallization and preliminary crystallographic analysis of Cg1458: A novel oxaloacetate decarboxylase from Corynebacterium glutamicum. Acta Crystallogr Sect F Struct Biol Cryst Commun. 2011; 67:968–970.
44. Highbarger LA, Gerlt JA, Kenyon GL. Mechanism of the reaction catalyzed by acetoacetate decarboxylase. Importance of lysine 116 in determining the pKa of active-site lysine 115. Biochemistry. 1996; 35:41–6. [PubMed: 8555196]
45. Burgi HB, Dunitz JD, Shefter E. Geometrical reaction coordinates. II. Nucleophilic addition to a carbonyl group. J Am Chem Soc. 1973; 95:5065–5067.
46. Burgi HB, Dunitz JD, Lehn JM, Wipff G. Stereochemistry of reaction paths at carbonyl centres. Tetrahedron. 1974; 30:1563–1572.
47. Timm DE, Mueller HA, Bhanumoorthy P, Harp JM, Bunick GJ. Crystal structure and mechanism of a carbon-carbon bond hydrolase. Structure. 1999; 7:1023–33. [PubMed: 10508789]
48. Karplus PA, Diederichs K. Linking crystallographic model and data quality. Science. 2012; 336:1030–3. [PubMed: 22628654]
49. Heinig M, Frishman D. STRIDE: a web server for secondary structure assignment from known atomic coordinates of proteins. Nucleic Acids Res. 2004; 32:W500–2. [PubMed: 15215436]
50. Brouns SJJ, Barends TRM, Worm P, Akerboom J, Turnbull AP, Salmon L, et al. Structural Insight into Substrate Binding and Catalysis of a Novel 2-Keto-3-deoxy-d-arabinonate Dehydratase Illustrates Common Mechanistic Features of the FAH Superfamily. J Mol Biol. 2008; 379:357–371. [PubMed: 18448118]

Europe PMC Funders Author Manuscripts

Europe PMC Funders Author Manuscripts

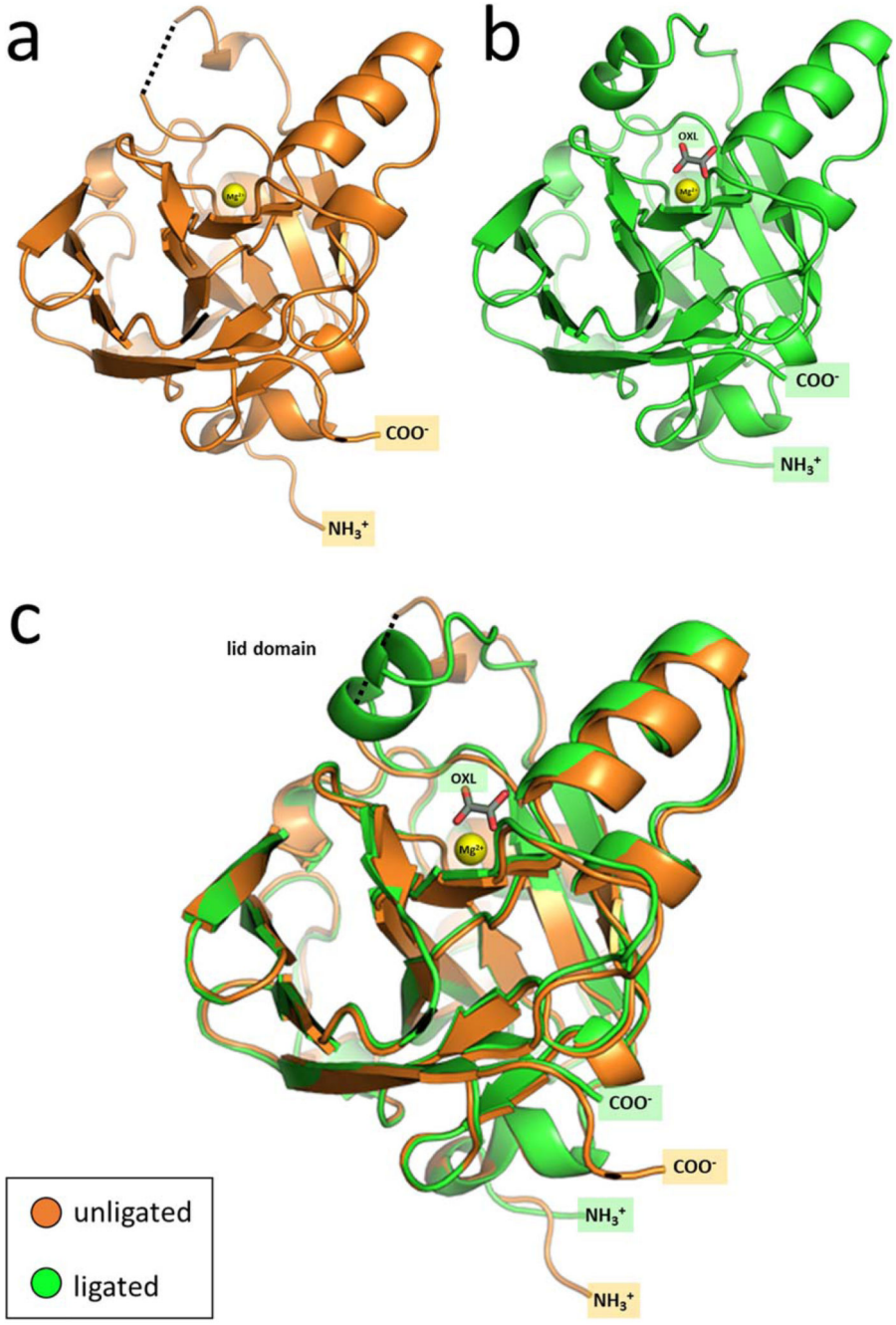

Figure 1. Alignment of FAHD1 crystal structures.

Structural comparison of human FAHD1 in its *unligated* (orange, **panel a**) and *ligated* (green, **panel b**) form. The catalytic center contains a magnesium ion (yellow sphere), the bound ligand oxalate (OXL) is displayed in **b**. Superposition of the free and the ligated form is shown in **Panel c**, demonstrating the high degree of similarity of the two structures, except for an *N*-terminal region referred to as flexible lid.

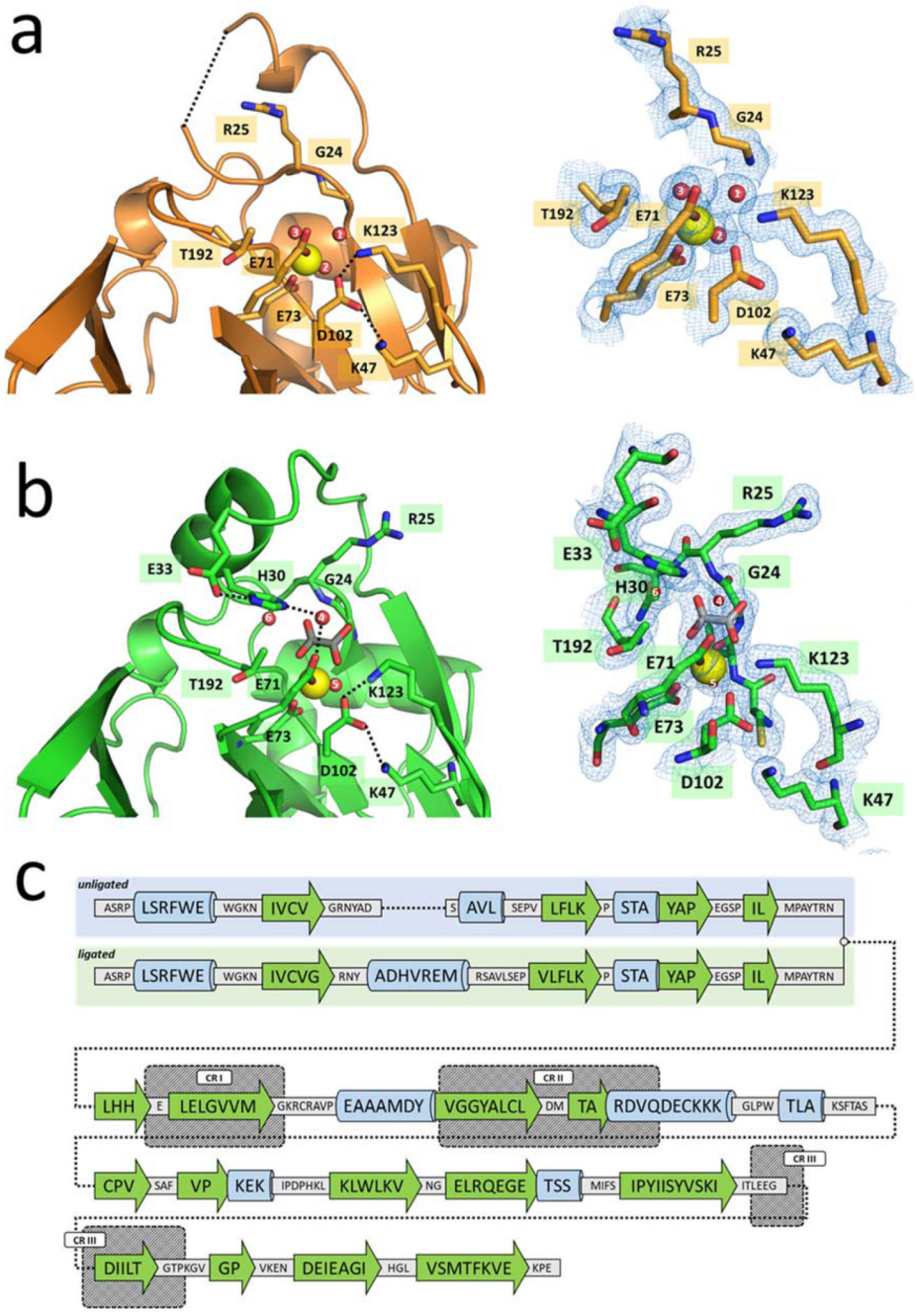

Figure 2. A detailed view of the catalytic center of FAHD1.

Panel a: Left: Detail view of the *unligated* structure. The inner coordination sphere of the magnesium ion (yellow sphere) is constituted by carboxylates of E71, E73, and D102, as well as by three water molecules (red spheres, labelled 1, 2, 3). The outer coordination sphere is constituted by G24, R25, K47, R106, Q109, and K123. **Right:** The corresponding 2*m*Fo-*D*Fc maximum likelihood electron density map is depicted as blue grid at the 0.5 sigma level.

Panel b: Left: Detail view of the *ligated* structure. Upon oxalate binding the coordination of the magnesium ion is altered: Two water molecules of the inner coordination sphere are replaced by oxygens from the ligand. Subsequently, the dyad E33-H30 of the lid region is positioned close to the magnesium ion. Water molecule 6 is stabilized by H30-E33 and E71. According to our model, water molecule 5 coordinates to the magnesium ion, whereas water molecule 6 is of minor importance for the architecture and function of the active site. **Right:** The corresponding 2*m*Fo-*D*Fc maximum likelihood electron density map is depicted as blue grid at the 1.2 sigma level.

In both views of panels a and b R106 is not displayed, to enable the undisturbed view into the catalytic center. (dashed lines: hydrogen bonding indicated by short acceptor-donor distances)

Panel c: A cartoon of secondary structure elements of *unligated* and *ligated* human FAHD1, extracted via STRIDE[49] from the structure data that we submitted into the PDB (6FOG, 6FOH). Green arrows represent β-sheets, blue cylinders represent α-helices and grey bars indicate loose loop structures. The three conserved regions (CR I, CR II, CR III) that comprise the evolutionary conserved FAH fold are denoted as grey rectangles. They are connected via hydrogen bond networks to constitute the enzyme cavity.

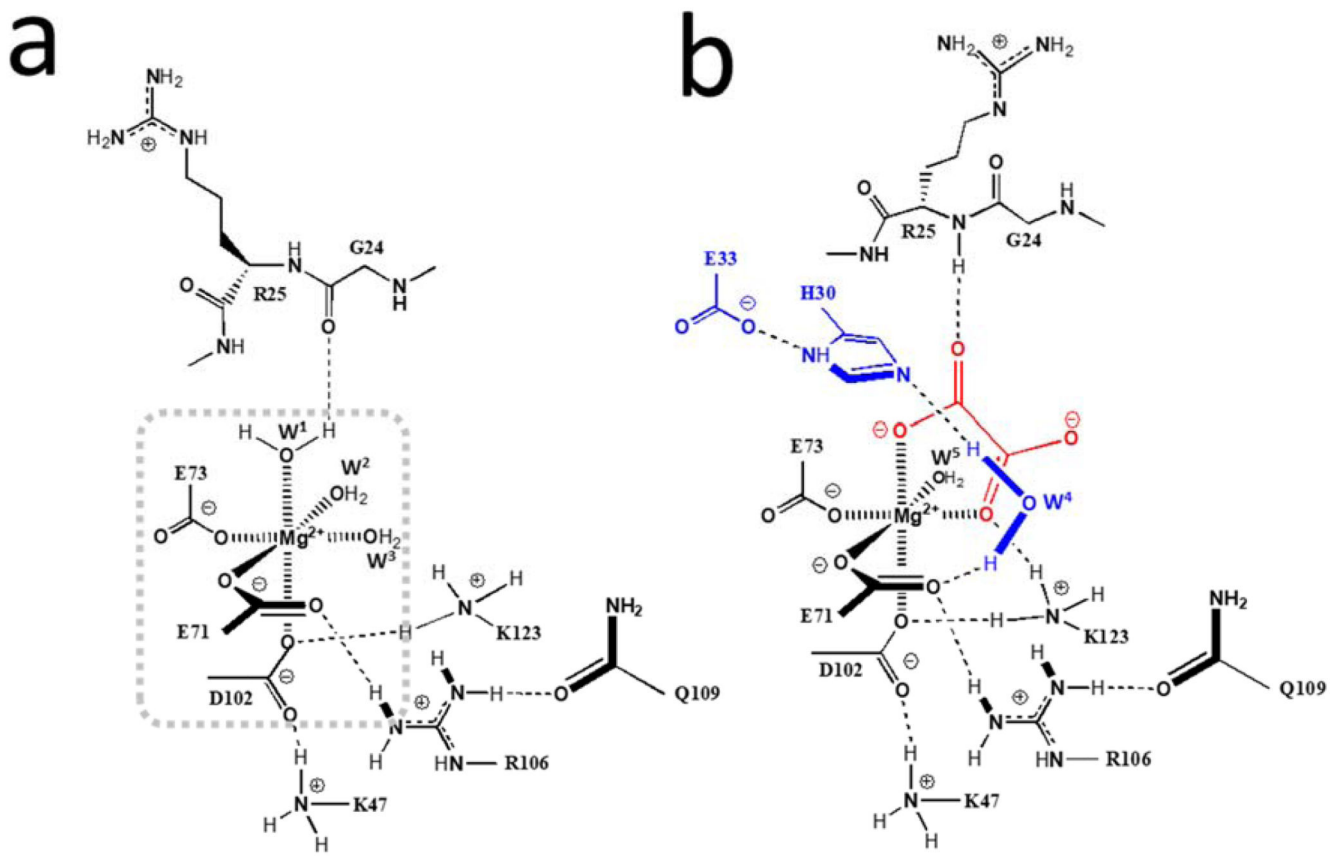

Figure 3. Chemical sketch of the catalytic sites of the *unligated* and *ligated* structures.

Panel a: In the *unligated* structure, the magnesium ion adopts an octahedral geometry. Three carboxylates (E73, E71, and D102) and three water molecules constitute the inner coordination sphere of the cofactor (dashed gray box). R106 is connected to E71 and Q109 by a hydrogen bond network. Side chains of K47 and K123 stabilize the side chain carboxylate of D102. The water molecule apical to D102 (water molecule 2 in Fig. 3a) operates as strong hydrogen donor to the amide carbonyl of G24.

Panel b: In the *ligated* structure, the FAHD1 inhibitor oxalate is bound to the cofactor in the catalytic center. The hydrogen bonding networks K47-D102-K123 and E71-R106-Q109, already established in the *unligated* structure (panel a), are not significantly affected by oxalate binding as indicated by only small changes in the hetero-atom distances of the hydrogen bond network. Oxalate (displayed in red) coordinates in a bidentate manner to the magnesium ion, thereby displacing two water molecules. Repulsive electron density is placed into the space of the G24 carbonyl oxygen, for which G24 performs a peptide-in plane-flip. The hydrogen bond acceptor character in the *unligated* structure *via* G24 is inverted into a strong hydrogen bond donor character *via* R25 in the *ligated* structure. Water molecule 6 in the ligated structure is not displayed in this picture, as it is not part of our model description.

(dashed lines: hydrogen bonding indicated by short acceptor-donor distances)

Europe PMC Funders Author Manuscripts

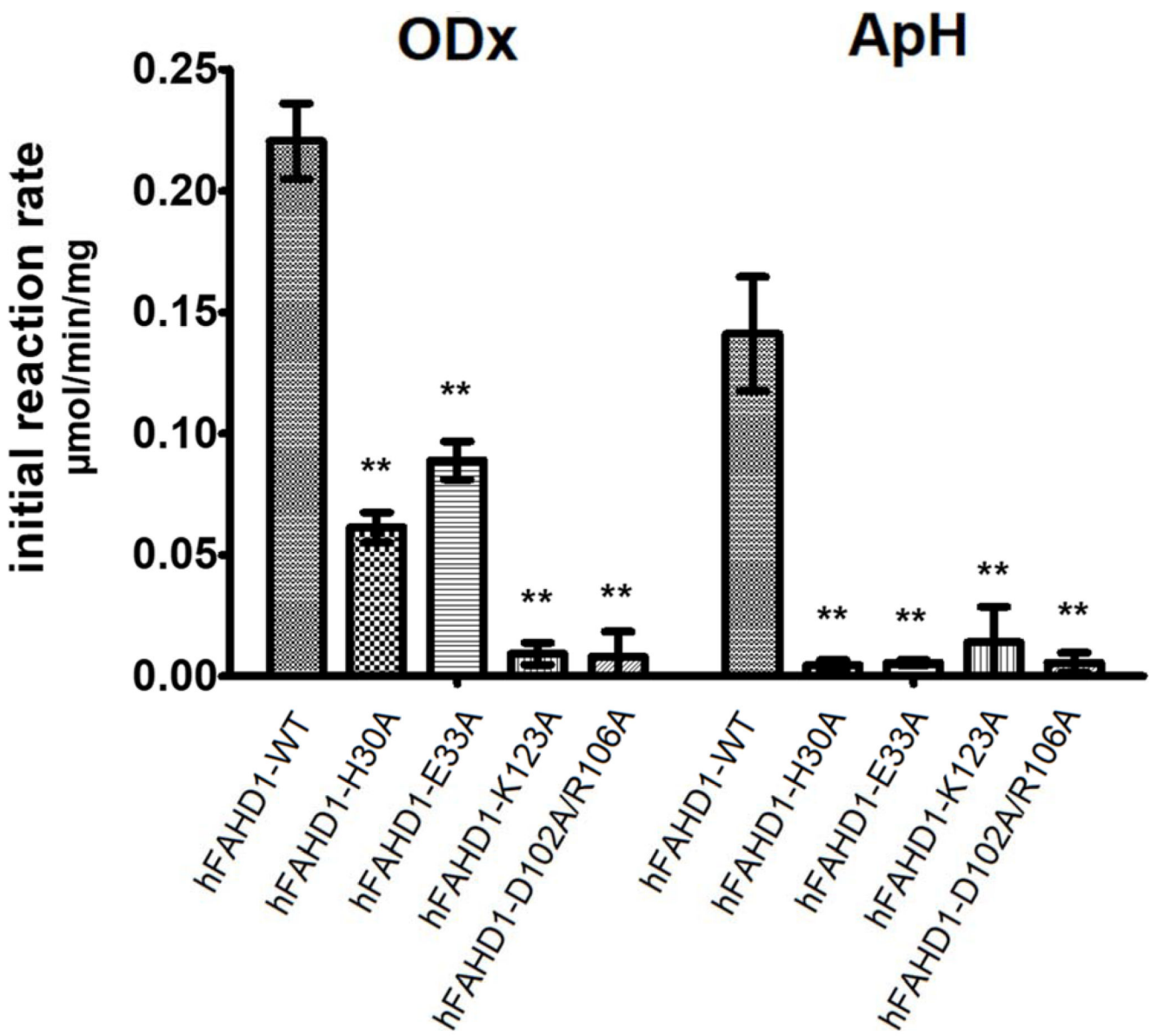

Figure 4. FAHD1 activity of selected point-mutants

Human FAHD1 proteins (hFAHD1) harboring selected point-variants were expressed in *E. coli* and purified by chromatographic techniques. The recombinant proteins were tested for ODx and ApH activity. Substitution of key amino acids identified by structural analysis of the FAHD1 ligand binding site caused loss of ApH activity in all cases whereas ODx activity was remained in the case of H30 and E33 variants confirming a different function of those residues in the two catalytic mechanisms. Kinetic data for this diagram in 300 µl of assay volume is provided in Tab. 3 in the main text. Error bars represent the standard deviation (n = 3) within 95 % of confidence interval. Student t-tests of significance were performed with respect to the wild-type data (** $p < 0.01$).

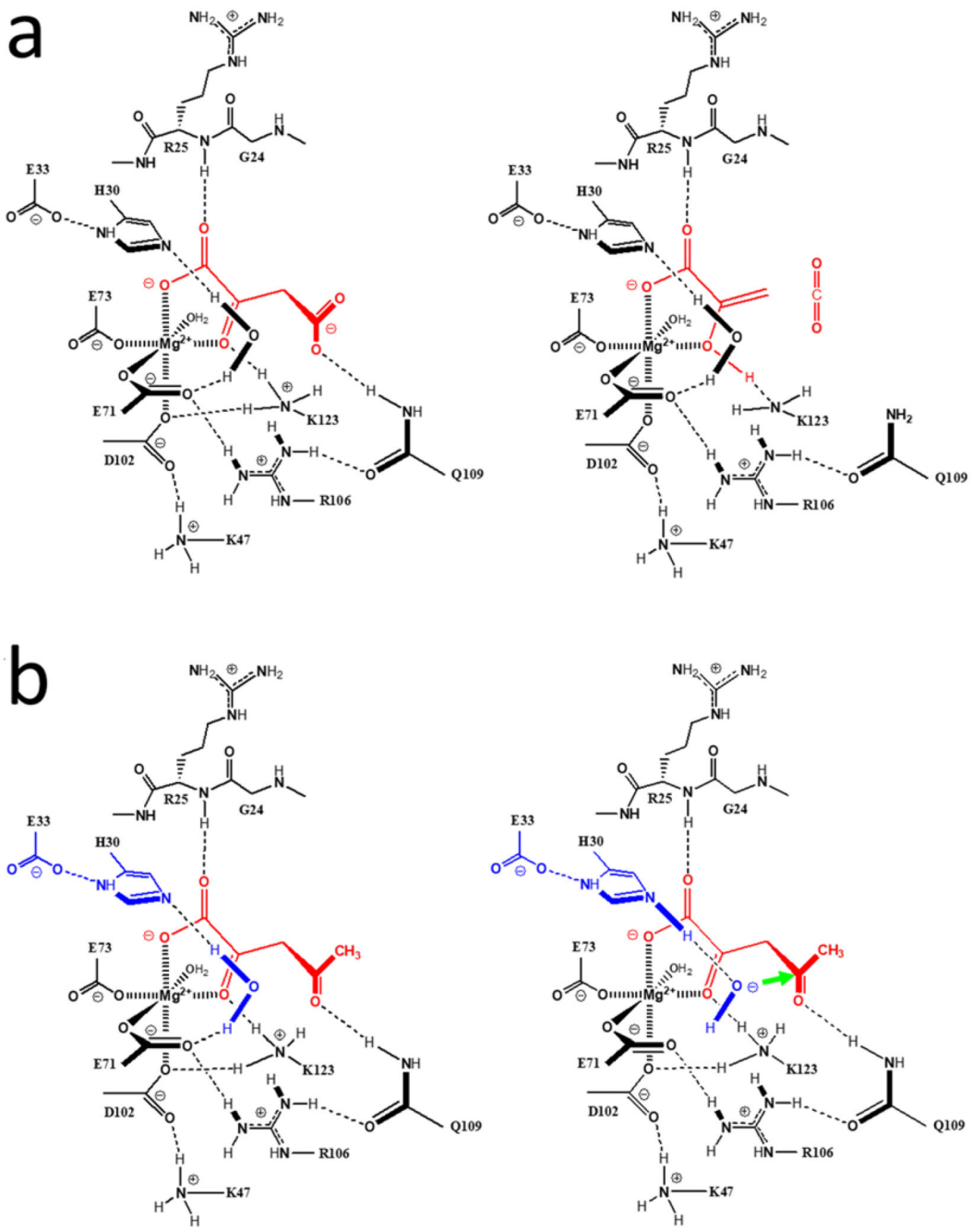

Figure 5. FAHD1 as ODx and ApH

(a): Left: Conformational control of Mg^{2+}-bound 2-keto oxaloacetate (red) by hydrogen bonding to Q109. **Right**: Decarboxylation and protonation of Mg^{2+}-bound pyruvate enolate by K123. The primary products of the C^3-C^4 bond cleavage in the decarboxylase process are enol pyruvate and carbon dioxide (red).

(b) Left: Generation of the hydroxyl nucleophile by deprotonation of the cavity-water molecule by assistance of the E33-H30 dyad (blue). Bound acetylpyruvate in red. **Right**: Nucleophilic attack of hydroxyl to the electrophilic C^4 of the acetyl group (green arrow),

followed by K123 assisted formation of hypothesized intermediate enol pyruvate and an acetic acid moiety.

Europe PMC Funders Author Manuscripts

Europe PMC Funders Author Manuscripts

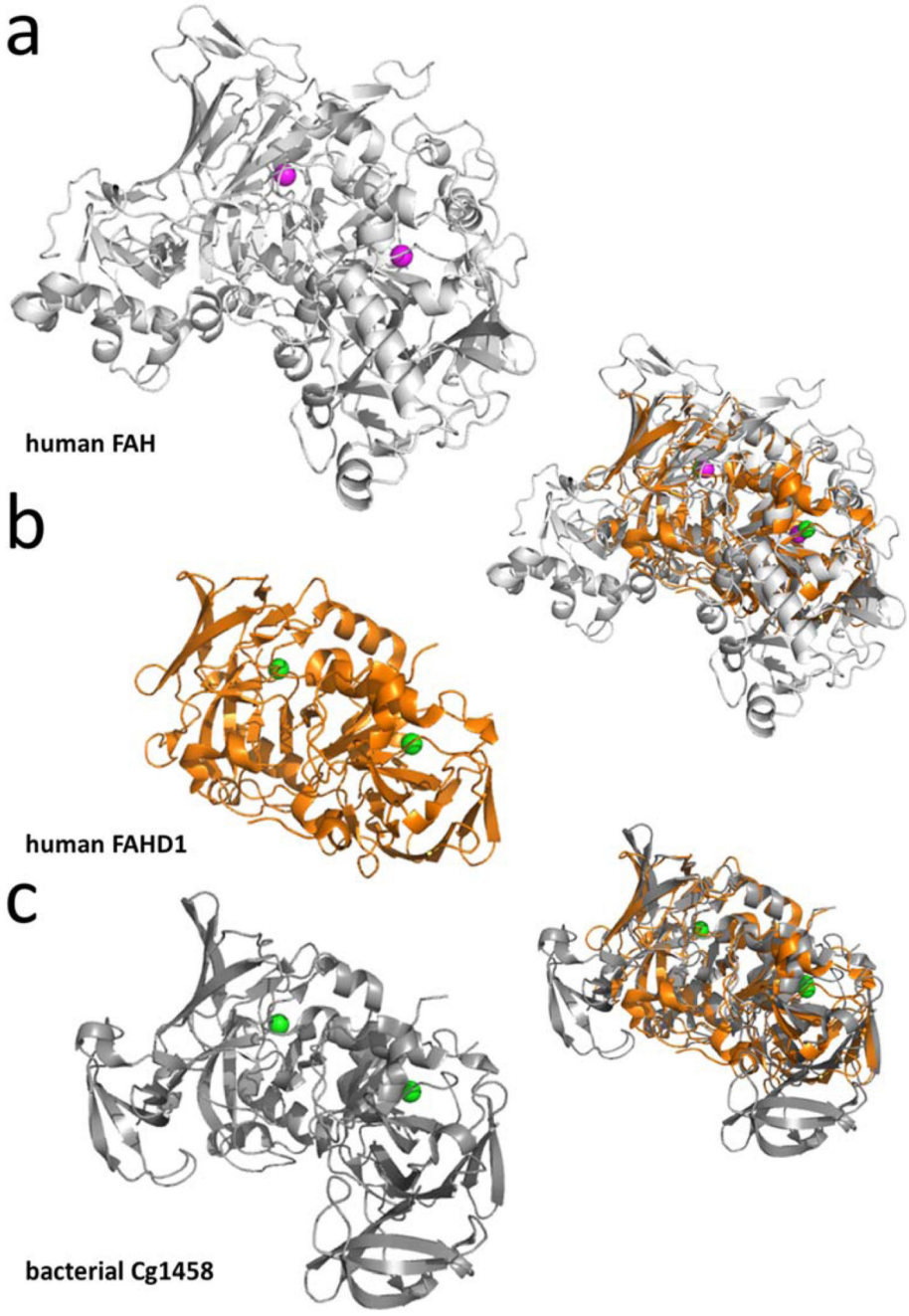

Figure 6. A structural comparison of FAH, FAHD1 and Cg1458.

Dimer structures of three similar members of the FAH superfamily depicted in cartoon shading. Ca^{2+} ions are depicted as violet spheres, and Mg^{2+} ions are displayed in green for a better contrast. **Panel a:** The crystal structure of unligated human fumarylacetoacetate hydrolase (hFAH) (PDB: 1QCN), as described by Timm et al[47]. **Panel b:** The crystal structure of unligated fumarylacetoacetate hydrolase domain containing protein 1 (hFAHD1) (PDB: 6FOH), as described in this work. **Panel c:** The crystal structure of the prokaryotic ODx Cg14583 of *Corynebacterium glutamicum* (PDB: 4DBF), as described by Ran et al[38].

In between the panels, right hand side: Structure /sequence alignment of FAHD1 with FAH and Cg1458, respectively. A more concise comparison may be found elsewhere[5,50].

Europe PMC Funders Author Manuscripts

Table 1

Data collection and processing

Diffraction source	**European Synchrotron Radiation Facility (ID30A-1) MASSIF-1**	
PDB code	**6FOH** (unligated)	**6FOG** (ligated)
Wavelength (Å)	0.966	0.966
Temperature (K)	100	100
Detector	Pilatus3_2M	Pilatus3_2M
Crystal-detector distance (mm)	183.0	247.6
Rotation range per image (°)	0.10	0.05
Total rotation range (°)	129	116
Spacegroup	$P2_12_12_1$	$P2_1$
a, b, c (Å)	44.0, 77.8, 119.9	75.8, 116.5, 125.4
α, β, γ (°)	90.0	90.0, 89.9, 90.0
Mosaicity (°)	0.20	0.13
Resolution range (Å)	65.3-1.56 (1.6-1.56)	100.0-1.94 (2.05-1.94)
Total No. of reflections	276,946 (20,203)	354,385 (53,786)
No. of unique reflections	58,013 (4,116)	154,275 (23,411)
Completeness (%)	97.9 (95.7)	94.3 (88.8)
$\langle I/\sigma(I)\rangle$	13.4 (2.0)	6.4 (1.17)
$\boldsymbol{R}_{\text{meas}}$[†]	**7.1 (83.0)**	**13.6 (100.5)**
$CC_{½}$	99.9 (51.8)	99.1 (58.3)
Overall *B* factor from Wilson plot (Å^2)	26.4	36.2

[†] $R_{meas} = (\sum_{hkl} (n/n-1)^{½} \sum_i |I_i(hkl)-<I(hkl)>|)/\sum_{hkl} \sum_i I_i(hkl)$, where $I_i(hkl)$ is the i^{th} of n observations of reflection hkl and $<I(hkl)>$ is the weighted average intensity for all observations of reflection hkl. Values for the outer shell are given in parentheses.

Europe PMC Funders Author Manuscripts

Table 2

Refinement statistic table

Refinement		***unligated***	***ligated***
R_{work} (%)		16.2	18.1
R_{free} (%)		18.9	20.8
RMSDs			
Bonds (Å)		0.0118	0.0128
Angles (°)		1.534	1.624
***B* factors in refinement**			
Proteins	chain A	24.4	28.6
	chain B	24.3	28.7
	chain C	*none*	28.8
	chain D	*none*	28.8
	chain E	*none*	28.7
	chain F	*none*	32.0
	chain G	*none*	29.7
	chain H	*none*	33.8
Ligands	*oxalate*	*none*	26.3
Water	H_2O	33.3	30.0
Metal ions	Mg^{2+}	15.9	32.7
	Cl^-	19.1	27.6
Model quality Ramachandran analysis (%)			
Most favored		97.37	98.77
Allowed		2.39	1.23
Outliers		**0.24**	**0.00**

Table 3
Kinetic parameter statistic table of hFAHD1 point-variants

	ODx					
variants	**kcat (μmol/min/mg)**		**KM (μM)**		**kcat/KM (1/min/mg) ****	
hFAHD1-WT	**0.210**	*0.196 - 0.230*	**40.5**	*24.1 - 57.0*	**17.3**	*13.5 - 27.1*
hFAHD1-H30A	**0.060**	*0.059 - 0.064*	**81.9**	*59.4 - 104.3*	**2.4**	*2.1 - 3.3*
hFAHD1-E33A	**0.090**	*0.086 - 0.094*	**42.1**	*29.6 - 54.6*	**7.1**	*5.7 - 9.7*
hFAHD1-K123A	0.010	*0.005 - 0.014*	*n.a.*		*n.a.*	
hFAHD1-D102A/R106A	0.008	*0.008 - 0.018*	*n.a.*		*n.a.*	

	ApH					
variants	**kcat (μmol/min/mg)**		**KM (μM)**		**kcat/KM (1/min/mg) ****	
hFAHD1-WT	**0.142**	*0.117 - 0.165*	**22.8**	*3.3 - 42.3*	**20.7**	*13.0 - 118.7*
hFAHD1-H30A	0.005	*0.003 - 0.007*	*n.a.*		*n.a.*	
hFAHD1-E33A	0.006	*0.005 - 0.006*	*n.a.*		*n.a.*	
hFAHD1-K123A	0.014	*0.003 - 0.025*	*n.a.*		*n.a.*	
hFAHD1-D102A/R106A	0.006	*0.006 - 0.009*	*n.a.*		*n.a.*	

Michaelis-Menten kinetic parameters have been obtained for the listed hFAHD1 pointvariants in 300 μl of assay buffer (**) (see Methods). The table presents average values and statistical ranges within 95 % confidence interval. Parameters and data statistics have been computed with *GraphPad Prism 5* via a non-linear least square fits to Michaelis-Menten plots. Figure S4 displays Michaelis-Menten plots for the ODx activities of hFAHDl-WT and the hFAHD1-H30A and E33A variants. The wild type parameters for ODx and ApH have been described[3,17], and all variants are found to be dead for ApH, for which no KM can be obtained (*n.a.:* not applicable).